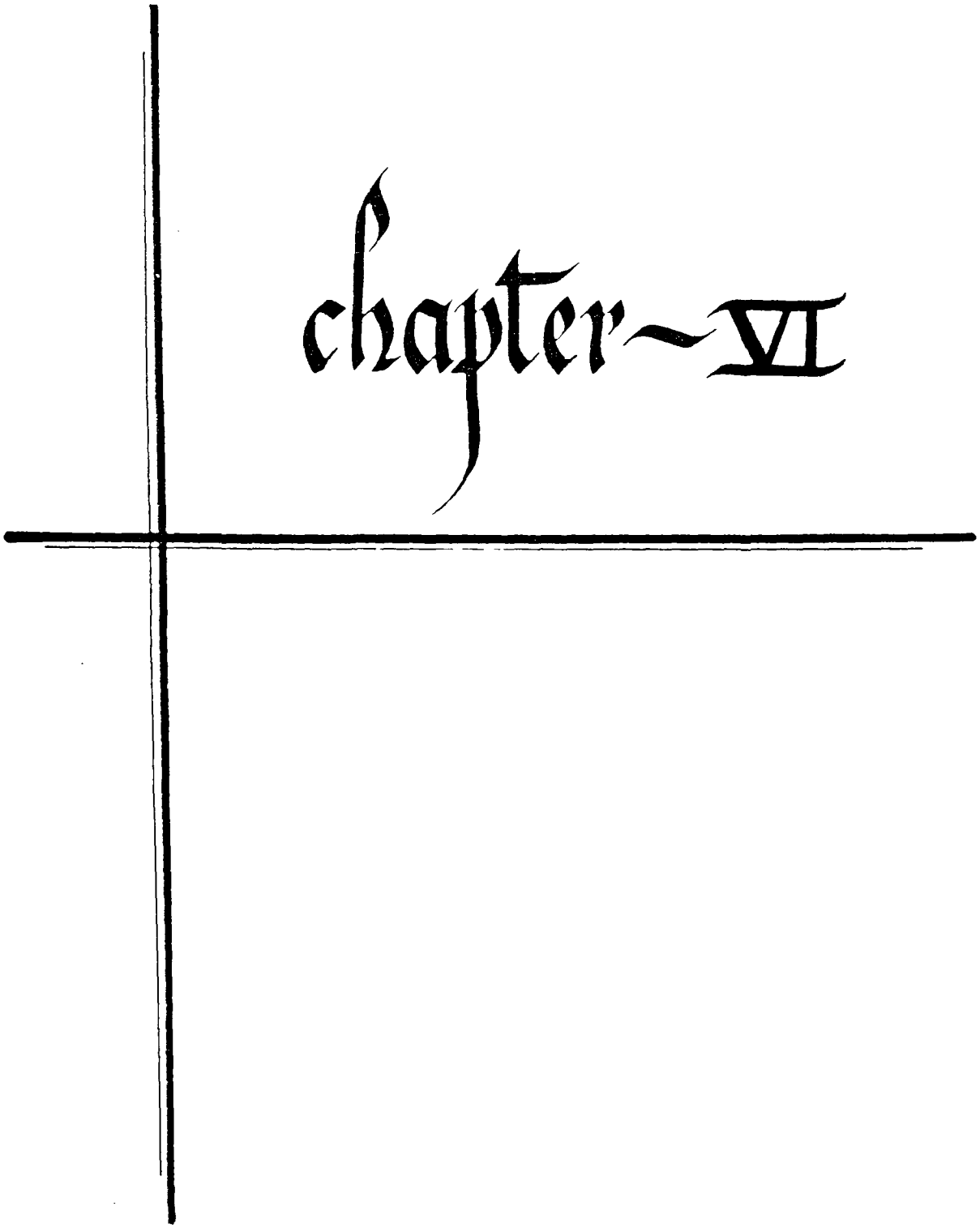
chapter~VI

CHAPTER VI

Direct current electrical conductivity study of the thermal decomposition of copper (II) oxalate monohydrate and zinc (II) oxalate dihydrate.

6.1 Introduction

Thermal analysis-thermogravimetry (TGA), differential thermogravimetry (DTG) and differential thermoanalysis (DTA) are widespread and helpful instruments in the hands of the chemist to reveal the energies of phase transition and chemical reactions, the thermal stabilities of educts and products as well as the nature and consistency of gaseous reaction products. Of itself thermal analysis provides only weak clues pertaining to reaction mechanisms, especially to the broadness of DTG and DTA peaks, the various intermediates formed during this step could not be detected; further, the TGA curve exhibited continuous weight loss until crystallization to metal oxide occurred. This is the principal shortcoming of the method but can be overcome by use of direct current electrical conductivity, which allow the formation of intermediates of varying conductivity.

The thermal decomposition reactions of metal oxalates have been widely investigated [1-9] . The influence of the

atmosphere on the course of the thermal decomposition of oxalate were exothermic in character whereas the majority of such decomposition in an inert atmosphere were endothermic [10-16] . Doremicux and Boulle [17] have also determined the decomposition characteristics of manganese, iron, cobalt, zinc and copper oxalates in the air and nitrogen atmospheres and reported a shift to lower temperature when oxygen is present for iron, manganese and cobalt oxalates but not for zinc and copper oxalates. The thermal, spectral and magnetic studies of compounds of copper and zinc carboxylates have also been studied [18-21] .

We have been using the electrical conductivity techniques in the study of solid state decomposition reactions of different metal (II) carboxylates [22-24] and this chapter is a continuation of our earlier work. In this chapter we will report the thermal decomposition of copper (II) oxalate monohydrate and, zinc (II) oxalate dihydrate have been studied using two-probe d.c. electrical conductivity measurements to study the progress of reaction. This study has been supplemented with TGA, DTG and DTA, X-ray diffraction and infrared spectroscopy.

6.2 Experimental

The procedure for synthesis of copper (II) oxalate

monohydrate ($CuC_2O_4 \cdot H_2O$) and zinc (II) oxalate dihydrate ($ZnC_2O_4 \cdot 2H_2O$) are given in chapter II. The experimental details for the determination of various physical properties viz. infrared spectrum, magnetic moment, thermal analyses (TGA, DTG and DTA), X-ray powder diffraction and direct current electrical conductivity are also explained in Chapter II.

6.3 Results and Discussion

6.3.1 Characterization of $CuC_2O_4 \cdot H_2O$ and $ZnC_2O_4 \cdot 2H_2O$

The results of the chemical analysis (Table I) show that there is a good agreement between found and calculated values of metal, carbon and hydrogen contents for the proposed formula $CuC_2O_4 \cdot H_2O$ and $ZnC_2O_4 \cdot 2H_2O$. The infrared spectrum (Fig. 1) showed frequencies corresponding to the carboxylate group, hydroxyl group, metal-oxygen, etc. and the assignments are made on the basis of earlier studies described in Chapter III. In all these complexes the metal has polymeric octahedral coordination [26,27] . The presence of water of crystallization was confirmed on the basis of the thermal analysis curve. The compound $CuC_2O_4 \cdot H_2O$ has magnetic moment of 1.96 B.M., while $ZnC_2O_4 \cdot 2H_2O$ has zero magnetic moment, which indicates that the compounds have the disorted octahedral stereochemistry.

6.3.2 Thermal decomposition processes of $CuC_2O_4 \cdot H_2O$ and $ZnC_2O_4 \cdot 2H_2O$

(a) Static air atmosphere

$CuC_2O_4 \cdot H_2O$

The TGA, DTG and DTA curves for $CuC_2O_4 \cdot H_2O$ are shown in Fig. 2(d). The dehydration of $CuC_2O_4 \cdot H_2O$ was indicated by the presence of one broad endothermic peak in the DTA and a peak at same temperature on DTG curve. The TGA curve showed a clear dehydration step corresponding to the loss of one water molecules from 105-200 ^{o}C (Calc., 10.62 %, found 11.01 %). The oxidative decomposition step was represented by a strong and broad peak on the DTA and DTG curve at 315 ^{o}C (Fig.2(a)). The TGA curve exhibited continuous weight loss until it crystallized to CuO (Calc., 47.51 %; found 48.00 %). Above 330 ^{o}C the lifting up weight loss was observed on TGA curve. This may be due to the non-stoichiometry (or defects) present in the final product.

The plot of log σ vs. T^{-1} in Fig. 2(b) showed a Region B at 83-182 ^{o}C for dehydration step. The isothermally heated sample of $CuC_2O_4 \cdot H_2O$ under static air, at 170 ^{o}C showed no H-OH bands in infrared spectrum. An additional band appeared at 798 cm^{-1} while other oxalate group bands observed

for the parent compound also showed a blue shift. The X-ray diffraction pattern (Fig. 3(b)) showed polycrystallinity of the sample with decrease in interplanar spacing (Table III) as compared to the parent compound (see Fig. 3(a); Table II). The elemental analyses were in good agreement with the formula CuC_2O_4. Region B of the plot of log σ vs. T^{-1} shown in Fig. 2(b) can be therefore related to dehydration of the oxalate. Such a change is probably associated with a change from the octahedral geometry of copper (II) to tetrahedral form.

After the dehydration step, the value of σ increased steadily from 182 to 240 ^{o}C (Region C). The infrared spectrum of the isothermally heated sample of $CuC_2O_4 \cdot H_2O$ at 215 ^{o}C showed a decrease in the intensities of coordinated carboxylate bands; in addition bands at 615 (s) cm^{-1} and 410 (m) cm^{-1} occurred for metal-oxygen stretching frequencies due to the presence of cuprous oxide [28] . The X-ray diffraction of this isothermally heated sample (Table IV) was generally broad (Fig. 3(c)). The pattern corresponded to anhydrous CuC_2O_4 and Cu_2O [29] . A sharp increase in the value of σ was observed within the temperature range 250-300 ^{o}C (Region D). For the sample heated isothermally at 280 ^{o}C, the infrared spectrum a weak band corresponding to the oxalate group, but

a strong band was observed at 400 cm^{-1}. The X-ray diffraction pattern of this isothermally heated sample was complex, probably corresponding to mixture of Cu_2O, CuC_2O_4 and CuO. Thus the steep increase in conductivity observed in Region D was due to the transformation of CuC_2O_4 to CuO, possibly via the semiconducting Cu_2O (about 10^{-6} ohm^{-1} cm^{-1}) [30] . Within the temperature range of Region E in Fig. 2(b), the value of σ remained almost constant. The sample obtained by heating isothermally in static air at 325 °C showed a black oxide. The X-ray diffraction pattern observed for this region indicated a predominance of CuO (Table V) [31]. No line which could be assigned to metallic copper was detected in our work. The sample thus obtained at 325 °C shows a change in σ as the temperature is changed.

$\underline{ZnC_2O_4 \cdot 2H_2O}$

Figure 2(c) showed the simultaneous TGA, DTG and DTA curves of $ZnC_2O_4 \cdot 2H_2O$. The DTA curve showed one endothermic peak at 145 °C and a peak in DTG was at 140 °C. The TGA curve at 110 °C showed a loss of 19.41 % and plateau up to 360 °C, indicating the elimination of two water molecules of crystallization (Calc. loss = 19.01 %). Thereafter, the decomposition was very rapid. The TGA curve showed a loss of 47.25 % of 375-425 °C corresponding to the formation of ZnO (Calc. loss = 46.94 %). This stage was supported by the

presence of an exothermic peak at 405 °C on the DTA curve and a peak at same temperature on DTG curve.

The temperature variation of the electrical conductivity σ in Fig. 2(d) showed a Region B at 70-250 °C corresponding to the dehydration step. The $ZnC_2O_4 \cdot 2H_2O$ sample, heated isothermally under static air at 200 °C, showed no H-OH bands in infrared spectrum and the X-ray diffraction pattern (Fig. 4(b)) was less crystalline (Table III) than the parent compound (see Fig. 4(a); Table II). The plot of log σ vs. T^{-1} (Fig. 2(d)) showed a steady increase in values of σ in the temperature range 250-410 °C (Region C). A sample heated isothermally in this region showed the infrared bands attributable to Zn-O stretching frequencies because more intense and those due to coordinated carboxylate decreased in intensity. The X-ray diffraction pattern (Fig. 4(c)) showed a generally sharp lines, indicating that the sample was predominantly crystalline. The pattern fits with the data for anhydrous zinc oxalate and zinc oxide (Table VI) [32].

A steep increase in σ was observed at 420 °C (Region D between 420 and 480 °C, Fig. 2(d)). The infrared spectrum and X-ray diffraction pattern (Fig. 4(d)) for the sample decomposed isothermally at 480 °C showed mainly ZnO (Table VII). The sample was white and had an electrical

conductivity value of about 10^{-3} ohm^{-1} cm^{-1} [33] . The sample thus obtained at 480 °C shows a variation in σ with temperature. This behaviour is characteristics of the non-stoichiometry present in ZnO [33,34] .

Thus the conventional thermal analysis (TGA, DTG and DTA) supplemented with electrical conductivity, infrared spectrum, X-ray diffraction patterns and elemental analyses gave a detailed analysis of the thermal decomposition of $CuC_2O_4 \cdot H_2O$ and $ZnC_2O_4 \cdot 2H_2O$. It is well known that the solid-state thermal decomposition of metal oxalates are influenced by the atmosphere [10-17] ; it was decided to undertake similar measurements in other controlled atmospheres.

(b) Dynamic nitrogen atmosphere

The TGA curve for $CuC_2O_4 \cdot H_2O$ in Fig. 5(a) showed a clear dehydration step corresponding to the loss of one water molecule from 90 to 210 °C, and this stage is supported by the presence of an endothermic peak at 170 °C on the DTA curve and a peak at same temperature on DTG curve. The decomposition of the oxalate (CuC_2O_4) was indicated by an endothermic peak in the DTA curve at 320 °C and in the DTG curve at 315 °C. This weight loss was found to be in good agreement with the formation of Cu_2O (Calc., 52.79 %; found, 53.08 %) as final product.

The plot of log σ vs. T^{-1} (Fig. 5(b)) showed that σ was initially constant, but then decreased steadily and remained constant up to 225 °C (Region B). The infrared spectrum, elemental analysis and X-ray diffraction pattern (similar to Fig. 3(b)) confirmed the formation of anhydrous copper oxalate in this region. After the dehydration step, the value of σ increased steadily within the temperature range 225-285 °C (Region C) and then a steep increase in σ at 285-320 °C (Region D). The X-ray diffraction pattern (Fig. 3(c)) and infrared spectrum for a sample heated isothermally in Region C showed a mixture of CuC_2O_4 and Cu_2O. The X-ray diffraction pattern (Fig. 3(c)) for a sample from the dry nitrogen atmosphere run obtained at 320 °C (Region D) showed sharp lines (Table VII) and was comparable with the data reported [29] for Cu_2O. The sample obtained at 320 °C showed a variation in σ with changing in temperature. This behaviour is characteristics of Cu_2O [30] . The sample was red in colour. Thus the X-ray diffraction patterns and conductivity measurements suggested that the product obtained by thermal decomposition of $CuC_2O_4 \cdot H_2O$ in a dry nitrogen atmosphere is pure Cu_2O, and that the concentration of copper metal, if present at all, is beyond the detection limit of these techniques.

$\underline{ZnC_2O_4 \cdot 2H_2O}$

The TGA, DTG and DTA curves of $ZnC_2O_4 \cdot 2H_2O$ are shown in Fig. 5(c). Dehydration of $ZnC_2O_4 \cdot 2H_2O$ was indicated by endothermic peak in the DTA and a peak in DTG curves at 150 °C. The TGA curve showed a weight loss with the range 80-170 °C, with a plateau upto 360 °C corresponding to the loss of two water molecules. The decomposition of the oxalate (ZnC_2O_4) was indicated by an endothermic peak in the DTA curve at 415 °C. The TGA curve showed a continuous weight loss 360-420 °C. This weight loss was found to be in good agreement with the formation of ZnO.

Region B in the plot of log σ vs. T^{-1} (Fig. 5(d)) corresponds to the dehydration of $ZnC_2O_4 \cdot 2H_2O$. There was a steep increase in σ at 320 °C followed by another steep increase at 417 °C (see Region C and D, in Fig. 5(d)). These two temperature ranges, 320-410 °C and 415-445 °C, can be tentatively assigned to the formation of zinc oxide together with some ZnC_2O_4 and ZnO, respectively. The X-ray diffraction and infrared spectrum were confirmed the formation of these phases. Thus the X-ray diffraction and conductivity measurements suggested that the product obtained by thermal decomposition of $ZnC_2O_4 \cdot 2H_2O$ in a nitrogen atmosphere is pure ZnO.

(c) Dynamic air atmosphere

$CuC_2O_4 \cdot H_2O$

In Fig. 6(a), for $CuC_2O_4 \cdot H_2O$, the DTA and DTG curves showed a peak at 160 °C for dehydration step, and TGA curve also produced a weight loss beginning at 100-190 °C corresponded to the removal of the water molecule contained in this oxalate. The broad exothermic peak corresponding to oxidative ~~oxidative~~ decomposition was shown on the DTA curve 310 °C and a peak at this temperature was also seen on the DTG curve. The TGA curve showed a continuous weight loss in this region, where the material finally crystallized to CuO. Supplementing the log σ vs. T^{-1} measurements (in Fig.6(b)) revealed the dehydration and the nature of the decomposition is similar to that shown in Fig. 2(b). The isothermal decomposition under a dynamic air atmosphere for $CuC_2O_4 \cdot H_2O$ at various temperature regions showed that the products obtained were similar to those from isothermally decomposing $CuC_2O_4 \cdot H_2O$ under a static air atmosphere.

$ZnC_2O_4 \cdot 2H_2O$

The TGA curve showed a weight loss between 85 and 155 °C (Fig. 6(c)). The DTA curve showed an endothermic peak at 135 °C and there was also a peak in the DTG curve at

same temperature, corresponding to the dehydration of $ZnC_2O_4 \cdot 2H_2O$, and an exothermic peak at 405 °C, corresponding to oxidative decomposition. The TGA showed a continuous weight loss from 380 °C until it crystallized to mainly ZnO.

The plot of log σ vs. T^{-1} in Fig. 6(d) was quite similar to Fig. 5(d). The infrared spectrum and X-ray diffraction pattern for the sample decomposed isothermally at Regions B, C and D were respectively anhydrous ZnC_2O_4, a mixture of ZnC_2O_4 and ZnO and pure ZnO in this atmosphere.

The prescribed intermediates obtained in each temperature region under all three atmospheres are shown in Tables VIII and IX.

The gases were collected at around 410 °C on the thermal decomposition of the parent compounds (i.e. $CuC_2O_4 \cdot H_2O$ and $ZnC_2O_4 \cdot 2H_2O$) under a dynamic nitrogen atmosphere. The qualitative gas analyses showed the presence of carbon monoxide and carbon dioxide. The detail detection procedure is described in Chapter III.

The different paths followed by the decomposition of $CuC_2O_4 \cdot H_2O$ and $ZnC_2O_4 \cdot 2H_2O$ in different atmospheres showed complete dehydration from conductivity measurements, thermal analyses (TGA, DTG and DTA) and the infrared spectrum.

A transformation of $CuC_2O_4 \cdot H_2O$ to CuO was detected in static and dynamic air atmospheres. These reactions are presented as follows :

$$CuC_2O_4 \cdot H_2O \xrightarrow{35\text{-}182\ ^{o}C} CuC_2O_4 + H_2O\uparrow \quad .. \quad (1)$$

$$2CuC_2O_4 \xrightarrow{182\text{-}240\ ^{o}C} Cu_2O + 3CO_2\uparrow + CO\uparrow \quad .. \quad (2)$$

$$Cu_2O + CuC_2O_4 \xrightarrow{240\text{-}320\ ^{o}C} 3CuO + 2CO\uparrow \quad .. \quad (3)$$

The transformation of CuC_2O_4 to Cu_2O was the final step detected in a dynamic dry nitrogen atmosphere, which ZnC_2O_4 transform to ZnO under static air, dynamic dry nitrogen and dynamic air atmospheres.

$$ZnC_2O_4 \cdot 2H_2O \xrightarrow{35\text{-}250\ ^{o}C} ZnC_2O_4 + 2H_2O\uparrow \quad .. \quad (4)$$

$$ZnC_2O_4 \xrightarrow{250\text{-}410\ ^{o}C} ZnO + CO\uparrow + CO_2\uparrow \quad .. \quad (5)$$

$$ZnC_2O_4 + ZnO \xrightarrow{410\text{-}560\ ^{o}C} 2\ ZnO + CO\uparrow + CO_2\uparrow \quad .. \quad (6)$$

6.4 Conclusions

The present study revealed following findings on the solid-state dehydration and decomposition of $CuC_2O_4 \cdot H_2O$ and $ZnC_2O_4 \cdot 2H_2O$.

(a) The dehydration of $CuC_2O_4 \cdot H_2O$ and $ZnC_2O_4 \cdot 2H_2O$ yielding anhydrous CuC_2O_4 or ZnC_2O_4, took place in all three of the atmospheres considered.

(b) In dry nitrogen, the formation of Cu_2O from $CuC_2O_4 \cdot H_2O$ was confirmed by using d.c. electrical conductivity measurements, in conjunction with infrared spectrum and X-ray diffraction investigations.

(c) The final product of decomposition in static air and dynamic air was found to be CuO for $CuC_2O_4 \cdot H_2O$. However, the final decomposition product in all three atmospheres was found to ZnO for $ZnC_2O_4 \cdot 2H_2O$.

(d) The oxidative behaviour of these oxalates was better understood from the study of temperature variation of d.c. electrical conductivity measurements.

6.5 References

1. D. Dollimore, Thermochim. Acta, 117 (1987) 331.
2. D. Dollimore, D.L. Griffiths and D. Nicholson, J. Chem. Soc. (1963) 2617.
3. D. Dollimore, J. Dollimore and D.Nicholson, J. Chem. Soc., (1962) 960.
4. J.V. Trojko and R.G. Nikola, Thermochim. Acta, 198 (1992) 360.
5. R. David, Bull. Soc. Chem. Fr., (1960) 717.
6. Ya. A. Uga, Z. Obshchei Khem, 24 (1954) 1315.
7. K. Kawagaki, J. Chem. Soc. Japan, 72 (1951) 1079.
8. F.A. Gooch and H.L. Ward, Am. J. Sci., 27 (1933) 448.
9. J. Robin, Bull. Soc. Chem. Fr., (1953) 1078.
10. D. Dollimore, J. Therm. Anal., 11 (1977) 185.
11. D.A. Young, 'Determination of Solids' (Pergamon Press, New York, 1966) P. 148.
12. W.E. Garner, 'Chemistry of the Solid State' (Butterworths Publ., 1955) P. 232.
13. D. Dollimore, J. Dollimore and J. Little, J. Chem. Soc., (1969) 2946.
14. M.Brown, D. Dollimore and A.K. Galwey, J. Chem. Soc. Farad. Trans. I, 70 (1974) 1316.
15. E.D. Macklen, J. Inorg. Nucl. Chem., 30 (1968) 2689.
16. C. Duval, 'Inorganic Thermogravimetric Analysis', (Elsevier, Amsterdam (1963)).

17. J.L. Doremicux and A. Boulle, C.R. Acad. Sci. Paris, 250 (1960) 3184.

18. J.R. Allan, B.R. Carson, D.L. Gerrard and S. Hoey, Thermochim. Acta, 147 (1989) 353.

19. J.A. Allan, G.M. Baillie, J.G. Bonner, D.L. Gerrard and S. Hoey, Thermochim. Acta, 143 (1989) 283.

20. K. Muraishi, K. Nagase and N. Tanaka, Thermochim. Acta, 23 (1978) 125.

21. A.A. Vecher, S.V. Dalidovich and E.A. Gusev, Thermochim. Acta, 89 (1985) 383.

22. K.S. Rane, A.K. Nikumbh and A.J. Mukhedkar, J. Mater Sci., 16 (1981) 2397.

23. A.K. Nikumbh, M.M. Rahman and A.D. Aware, Thermochim. Acta, 159 (1990) 109.

24. A.K. Nikumbh, A.E. Athare and V.B. Raut, Thermochim. Acta, 186 (1991) 217.

25. A.K. Nikumbh, A.A. Latkar and M.M. Phadke, Thermochim. Acta, 219 (1993) 269.

26. K. Nakamoto, 'Infrared and Raman Spectra of Inorganic and Coordination Compounds', (Wileys, New York, 1978).

27. N.F. Curtis, J. Chem. Soc. A, (1968) 1585.

28. J. Fujita, A.E. Martell and K. Nakamoto, J. Chem.Phys., 36 (1962) 324 and 331.

29. ASTM File Number 5-667.

30. A.P. Young and C.M. Schwartz, J. Phys. and Chem. Solids, 30 (1969) 249.

31. ASTM File Number, 5-661.

32. ASTM File Number, 5-664.

33. A.V. Krylova, L. Ya Margolis and G.I. Chizhikova, Kinetika Kataliz 6(5) (1965) 771 and 854.

34. W.J. Moore, 'Seven Solid States : An introduction to chemistry and physics of solids', (W.A. Benjamin, Inc., New York, 1967) P. 145.

Table I : Analytical data of copper (II) oxalate monohydrate ($CuC_2O_4 \cdot H_2O$) and zinc (II) oxalate dihydrate ($ZnC_2O_4 \cdot 2H_2O$)

Compound	Formula	Formula weight	Elemental analysis in wt. %						Magnetic moment (μ) B.M.
			C		H		Metal		
			Calc.	Found	Calc.	Found	Calc.	Found	
Copper (II) oxalate monohydrate (Colour - Light bluish green)	$CuC_2O_4 \cdot H_2O$	169.54	14.16	15.01	1.18	1.24	37.47	38.00	1.96
Zinc (II) oxalate dihydrate (Colour- - White)	$ZnC_2O_4 \cdot 2H_2O$	189.37	12.67	12.83	2.11	2.22	34.52	35.08	Dia-magnetic

Table II : X-ray diffraction data of $CuC_2O_4 \cdot H_2O$ and $ZnC_2O_4 \cdot 2H_2O$[a]

Observed d-spacing values (A^o) $CuC_2O_4 \cdot H_2O$	Observed d-spacing values (A^o) $ZnC_2O_4 \cdot 2H_2O$
4.66 (8)	4.67 (100)
3.86 (100)	3.86 (39)
2.80 (16)	3.56 (22)
2.49 (30)	2.96 (72)
	2.67 (23)
	2.63 (48)
	2.59 (28)
2.45 (25)	2.54 (46)
2.36 (19)	2.33 (20)
2.17 (12)	2.19 (40)
1.95 (24)	2.12 (23)
1.78 (36)	2.08 (13)
	2.00 (41)
1.71 (22)	1.97 (17)
1.62 (26)	1.90 (32)
1.56 (17)	1.85 (28)
1.52 (14)	1.77 (20)
1.48 (47)	1.68 (17)
	1.64 (16)
1.32 (10)	1.61 (23)
1.31 (12)	1.57 (18)
1.29 (8)	1.52 (32)
1.23 (11)	1.50 (8)
1.17 (8)	1.46 (16)
	1.35 (21)
	1.29 (18)
	1.21 (15)
	1.10 (26)

a. The figures given in the parentheses are intensities relative to the linewidth intensities (100).

Table III : X-ray diffraction data for anhydrous CuC_2O_4 and ZnC_2O_4 obtained from $CuC_2O_4 \cdot H_2O$ and $ZnC_2O_4 \cdot 2H_2O$ by heating in an atmosphere of nitrogen at 170 °C and 200 °C respectively[a]

Observed d-spacing for CuC_2O_4 (A^o)	Observed d-spacing for ZnC_2O_4 (A^o)
4.92 (14)	4.79 (10)
4.43 (12)	3.78 (100)
4.04 (100)	3.60 (18)
3.70 (14)	2.81 (32)
2.79 (14)	2.66 (28)
2.22 (23)	2.48 (20)
2.10 (31)	2.17 (10)
1.97 (18)	1.99 (19)
1.80 (14)	1.77 (21)
1.65 (27)	1.60 (25)
1.58 (8)	1.47 (30)
1.43 (9)	

[a] The figures given in the parentheses are intensities relative to the linewidth intensity (100).

Table IV : X-ray diffraction data for CuC_2O_4 and Cu_2O obtained from $CuC_2O_4 \cdot H_2O$ by heating in atmosphere of static air at 215 °C[a]

Observed d-spacing (A^o)	Cu_2O d-spacing[b] (A^o)
3.80 (72)	
3.56 (6)	
3.02 (11)	3.02 (9)
2.85 (21)	
2.63 (12)	
2.47 (100)	2.46 (100)
2.35 (9)	
2.20 (6)	
2.16 (45)	2.14 (37)
1.93 (5)	
1.66 (20)	
1.54 (35)	1.51 (27)
1.43 (8)	
1.31 (28)	1.29 (17)
1.20 (10)	1.23 (4)
	1.07 (2)
0.96 (8)	0.98 (4)
	0.95 (3)
	0.87 (3)
	0.82 (3)

[a] The figures given in parentheses are intensities relative to the linewidth intensity (100).

[b] Ref. No. 29.

Table V : X-ray diffraction data for CuO obtained from $CuC_2O_4 \cdot H_2O$ by heating in an atmosphere of static air at 325 ^oC[a]

Observed d-spacing (A^o)	CuO D-spacing (A^o)
2.75 (19)	2.75 (12)
2.55 (40)	2.53 (49)
2.53 (100)	2.52 (100)
2.33 (91)	2.32 (96)
2.28 (42)	2.31 (30)
1.88 (30)	1.87 (25)
1.73 (15)	1.71 (08)
1.57 (19)	1.58 (14)
1.50 (23)	1.50 (20)
1.41 (25)	1.42 (15)
1.38 (24)	1.37 (19)
1.29 (10)	1.30 (07)
	1.17 (05)
	1.09 (06)
	0.98 (04)

[a] The figures given in parenthese are intensities relative to the linewidth intensity (100).

[b] Ref. No. 31.

Table VI : X-ray diffraction data for ZnC_2O_4 and ZnO obtained from $ZnC_2O_4 \cdot 2H_2O$ by heating in an atmosphere of static air 480 ^oC[a]

Observed d-spacing (A^o)	ZnO d-spacing[b] (A^o)
2.83 (66)	2.82 (71)
2.63 (51)	2.60 (56)
2.46 (100)	2.48 (100)
1.92 (18)	1.91 (29)
1.63 (38)	1.63 (40)
1.48 (27)	1.48 (35)
1.41 (8)	1.41 (6)
1.38 (25)	1.38 (28)
1.35 (13)	1.36 (14)
	1.30 (3)
	1.24 (5)
	1.18 (3)
1.10 (8)	1.09 (10)
	1.06 (4)
1.02 (11)	1.04 (10)
	1.01 (5)
	0.98 (7)
0.89 (18)	0.91 (12)
	0.88 (6)
	0.84 (6)

[a] The figures given in parenthesis are intensities relative to the linewidth intensity (100).

[b] Ref. No. 32.

Table VII : X-ray diffraction data for Cu_2O and ZnO obtained from $CuC_2O_4 \cdot H_2O$ and $ZnC_2O_4 \cdot 2H_2O$ by heating in an atmosphere of nitrogen at 320 °C and 420 °C respectively[a]

Observed d-spacing for Cu_2O (A^o)	Observed d-spacing for ZnO (A^o)
2.98 (16)	2.84 (69)
2.47 (100)	2.59 (55)
2.16 (48)	2.46 (100)
1.50 (21)	1.93 (21)
1.32 (22)	1.62 (37)
1.23 (10)	1.47 (27)
1.05 (6)	1.40 (12)
0.97 (11)	1.37 (26)
0.90 (8)	1.35 (13)
	1.08 (15)
	0.99 (20)
	0.90 (22)

[a] The figures given in parenthese are intensities relative to the linewidth intensity (100).

Table VIII : Predicted intermediates and final product obtained from $CuC_2O_4 \cdot H_2O$ under different atmospheres, measured via d.c. electrical conductivity

Atmosphere	Regions	Temperature range, ^oC	Predicted intermediates and final product
Static air	A	25 - 83	$CuC_2O_4 \cdot H_2O$
	B	83 - 182	CuC_2O_4
	C	182 - 240	$CuC_2O_4 + Cu_2O$
	D	240 - 325	$CuC_2O_4 + Cu_2O + CuO$
	E	above 325	CuO
Dynamic nitrogen	A	25 - 50	$CuC_2O_4 \cdot H_2O$
	B	50 - 225	CuC_2O_4
	C	225 - 285	$CuC_2O_4 + Cu_2O$
	D	285 - 320	Cu_2O
Dynamic air	A	25 - 60	$CuC_2O_4 \cdot H_2O$
	B	60 - 200	CuC_2O_4
	C	200 - 260	$CuC_2O_4 + Cu_2O$
	D	260 - 310	$CuC_2O_4 + Cu_2O + CuO$
	E	above 310	CuO

Table IX : Predicted intermediates and final product obtained from $ZnC_2O_4 \cdot 2H_2O$ under different atmospheres, measured via d.c. electrical conductivity

Atmosphere	Regions	Temperature range, ^oC	Predicted intermediates and final product
Static air	A	25 - 70	$ZnC_2O_4 \cdot 2H_2O$
	B	70 - 250	ZnC_2O_4
	C	250 - 410	ZnC_2O_4 + ZnO
	D	410 - 480	ZnO
Dynamic nitrogen	A	25 - 80	$ZnC_2O_4 \cdot 2H_2O$
	B	80 - 320	ZnC_2O_4
	C	320 - 410	ZnC_2O_4 + ZnO
	D	410 - 445	ZnO
Dynamic air	A	25 - 75	$ZnC_2O_4 \cdot 2H_2O$
	B	75 - 310	ZnC_2O_4
	C	310 - 400	ZnC_2O_4 + ZnO
	D	400 - 450	ZnO

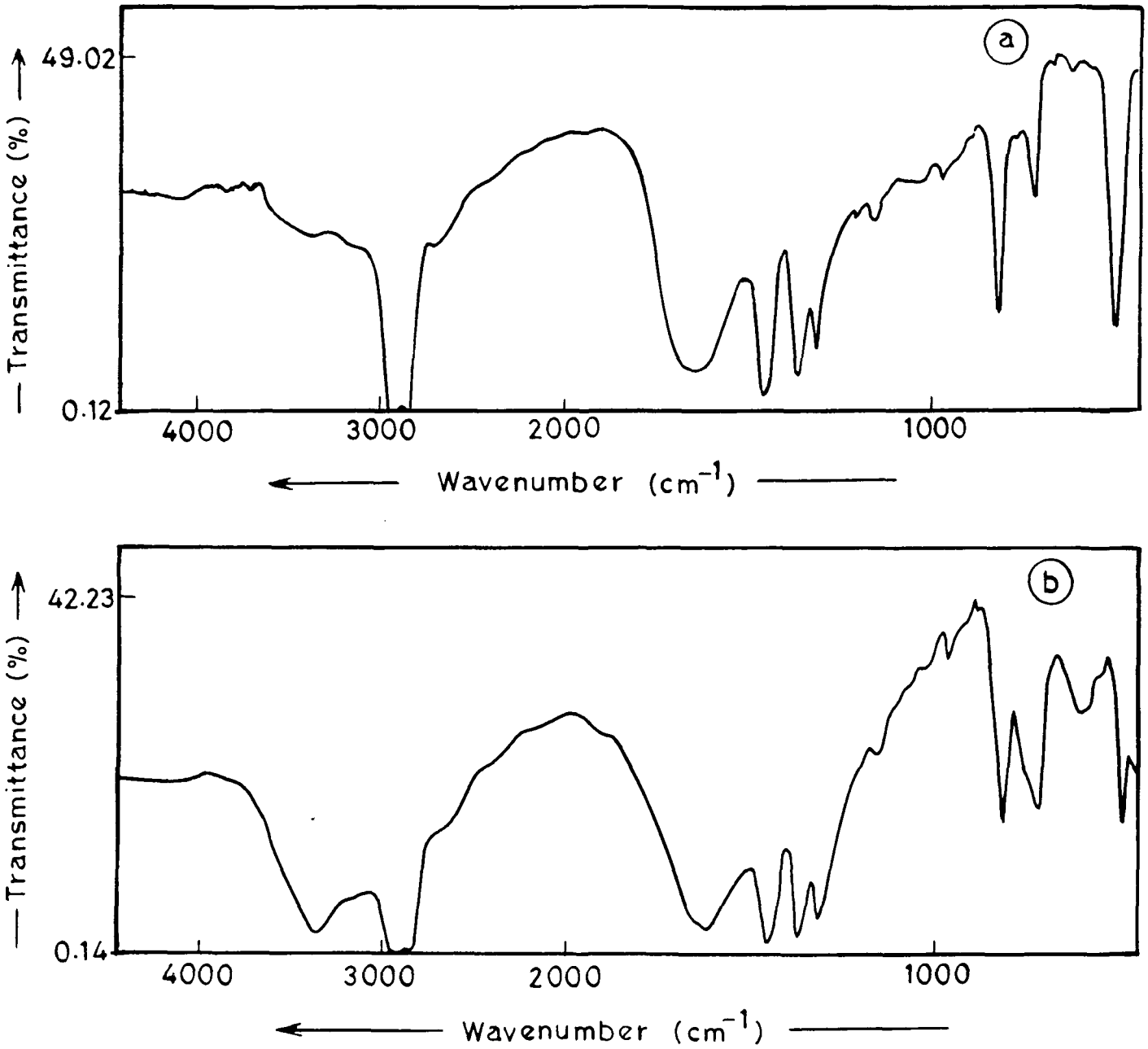

Fig. 1. Infrared spectra of (a) copper (II) oxalate monohydrate ($CuC_2O_4 \cdot H_2O$) and (b) zinc (II) oxalate dihydrate ($ZnC_2O_4 \cdot 2H_2O$).

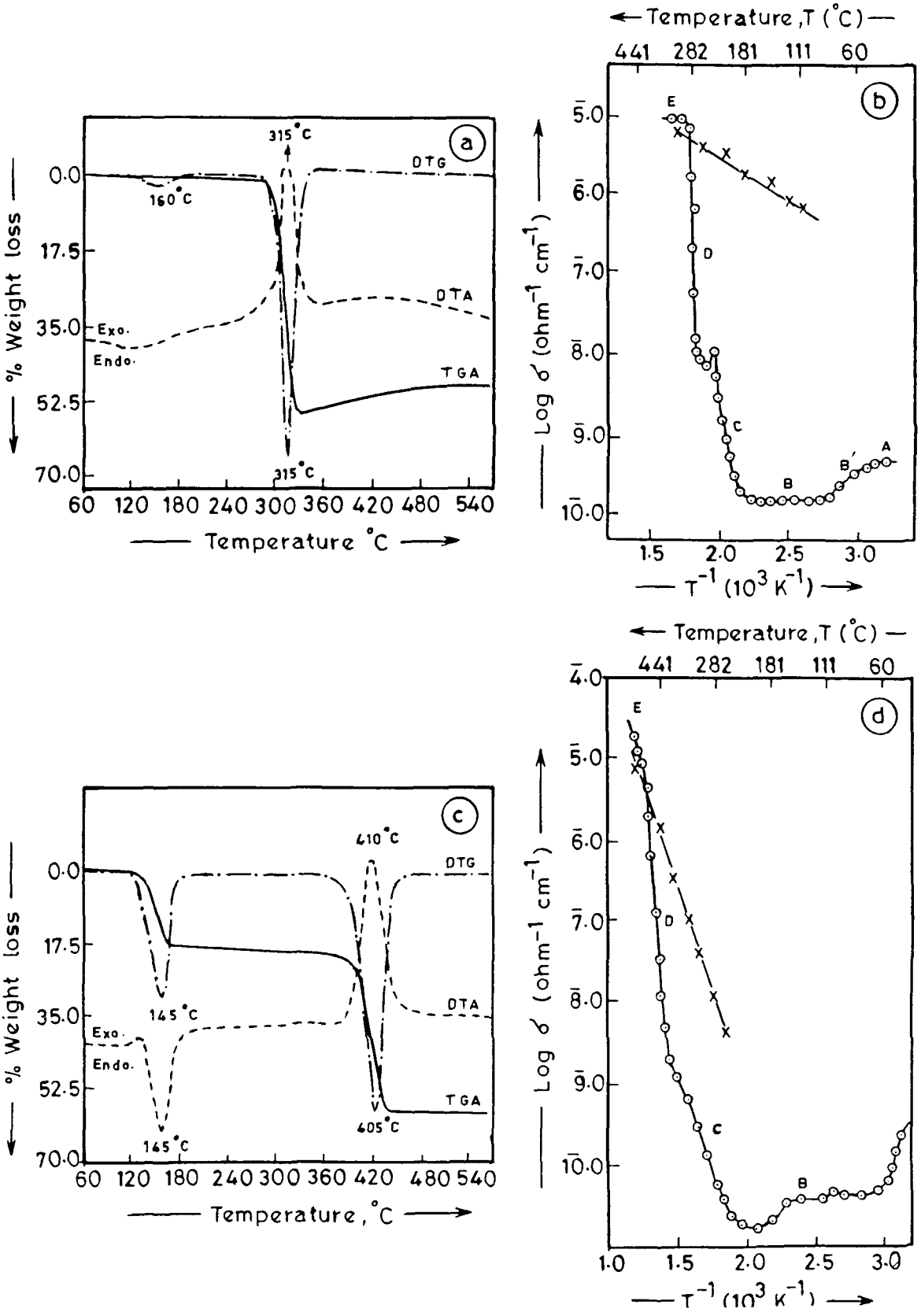

Fig. 2. Thermal decomposition in a static air atmosphere.
(a) TGA, DTG and DTA curves for $CuC_2O_4 \cdot H_2O$;
(b) Plot of log σ vs. T^{-1} for $CuC_2O_4 \cdot H_2O$:
⊙ during decomposition; X, cooling cycle;
(c) TGA, DTG and DTA curves for $ZnC_2O_4 \cdot 2H_2O$;
(d) Plot of log σ vs. T^{-1} for $ZnC_2O_4 \cdot 2H_2O$:
⊙ during decomposition; X cooling cycle.

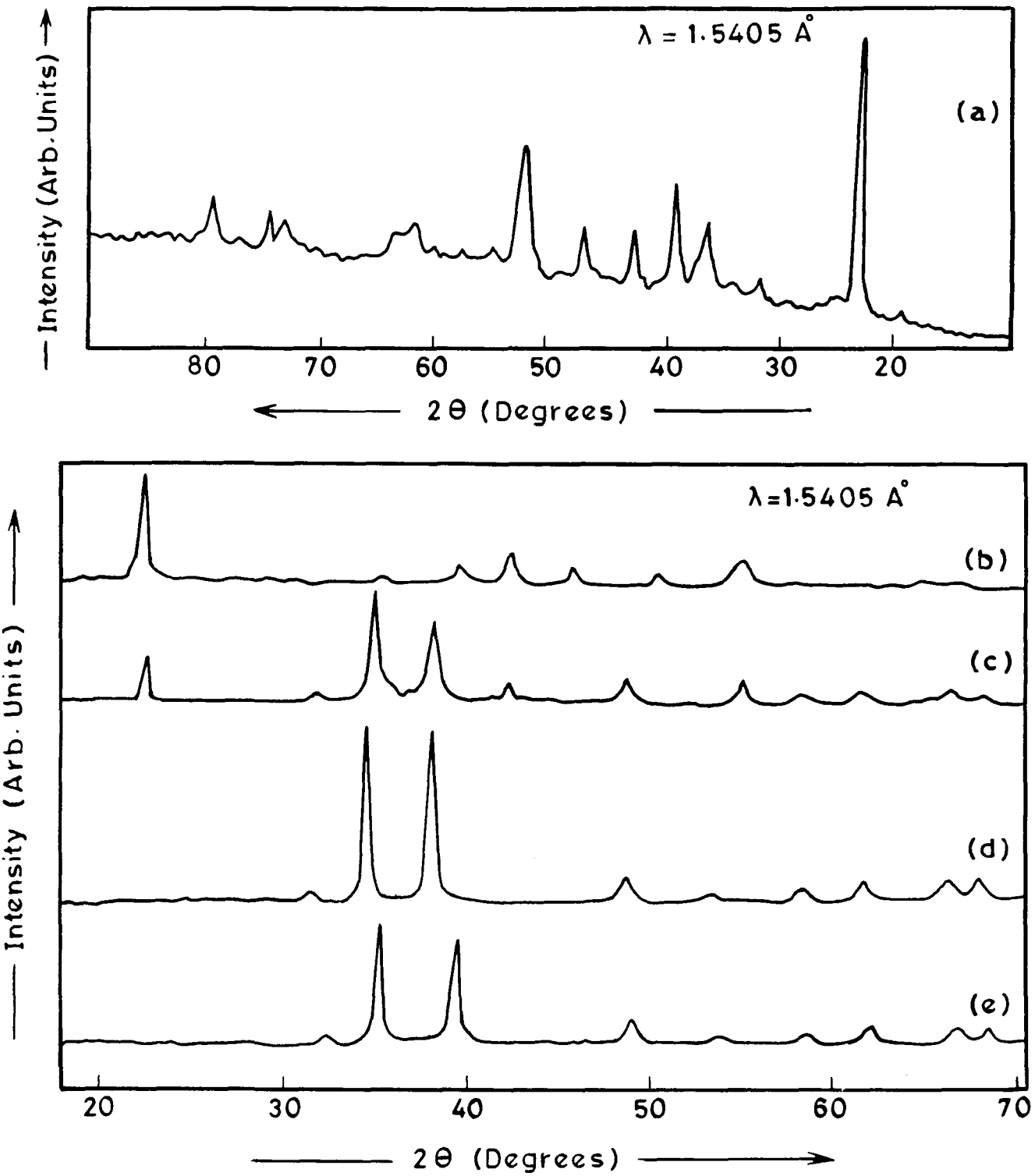

Fig. 3. X-ray diffraction patterns of copper (II) oxalate monohydrate ($CuC_2O_4 \cdot H_2O$) and its decomposed products at various temperatures. (a) $CuC_2O_4 \cdot H_2O$; (b) 170 °C; (c) 215 °C; (d) 325 °C; (e) 320 °C (nitrogen atmosphere).

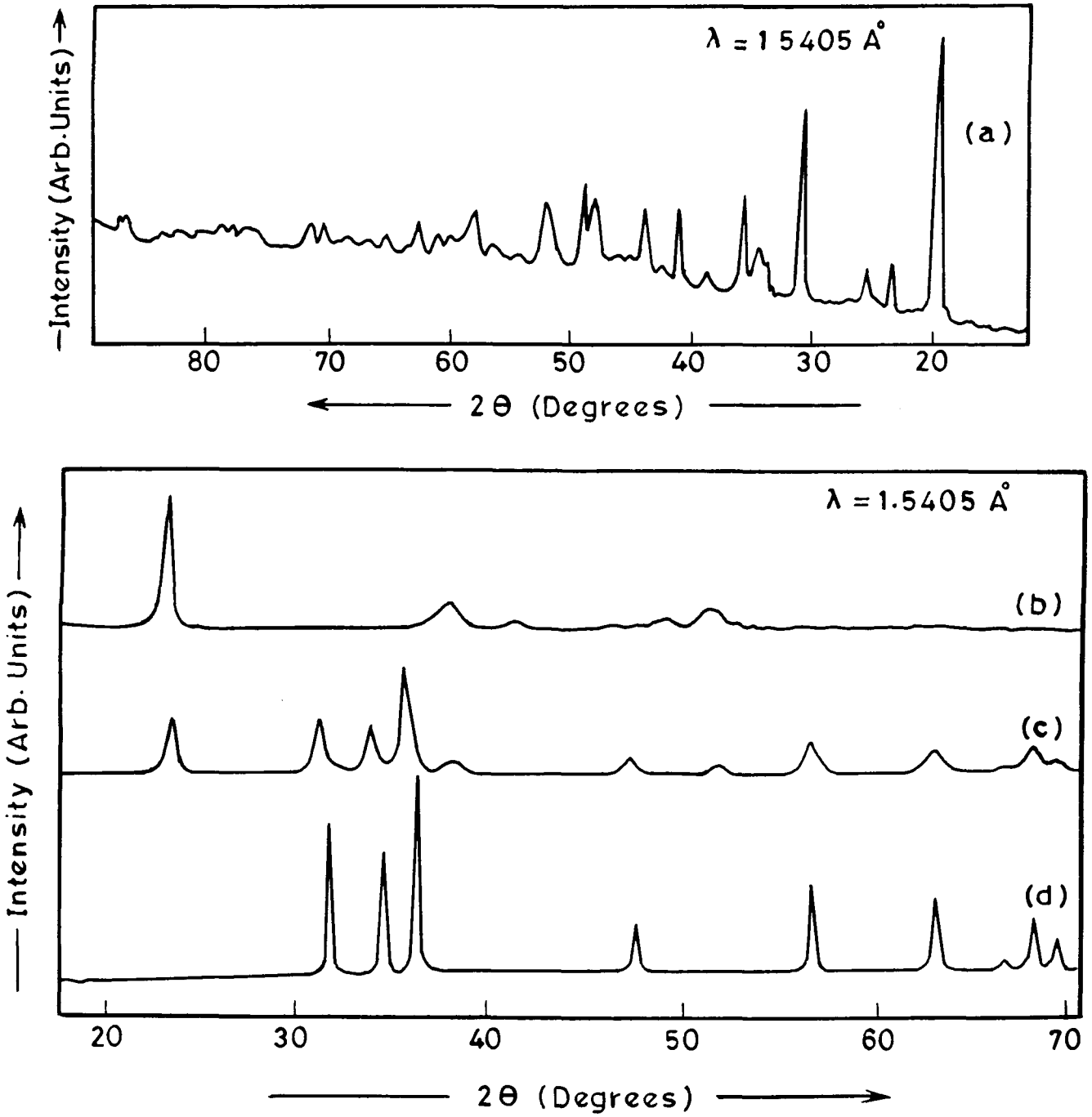

Fig. 4. X-ray diffraction patterns of zinc (II) oxalate dihydrate ($ZnC_2O_4 \cdot 2H_2O$) and its decomposed products at various temperatures. (a) $ZnC_2O_4 \cdot 2H_2O$; (b) 200 °C; (c) 480 °C; (d) 420 °C (nitrogen atmosphere).

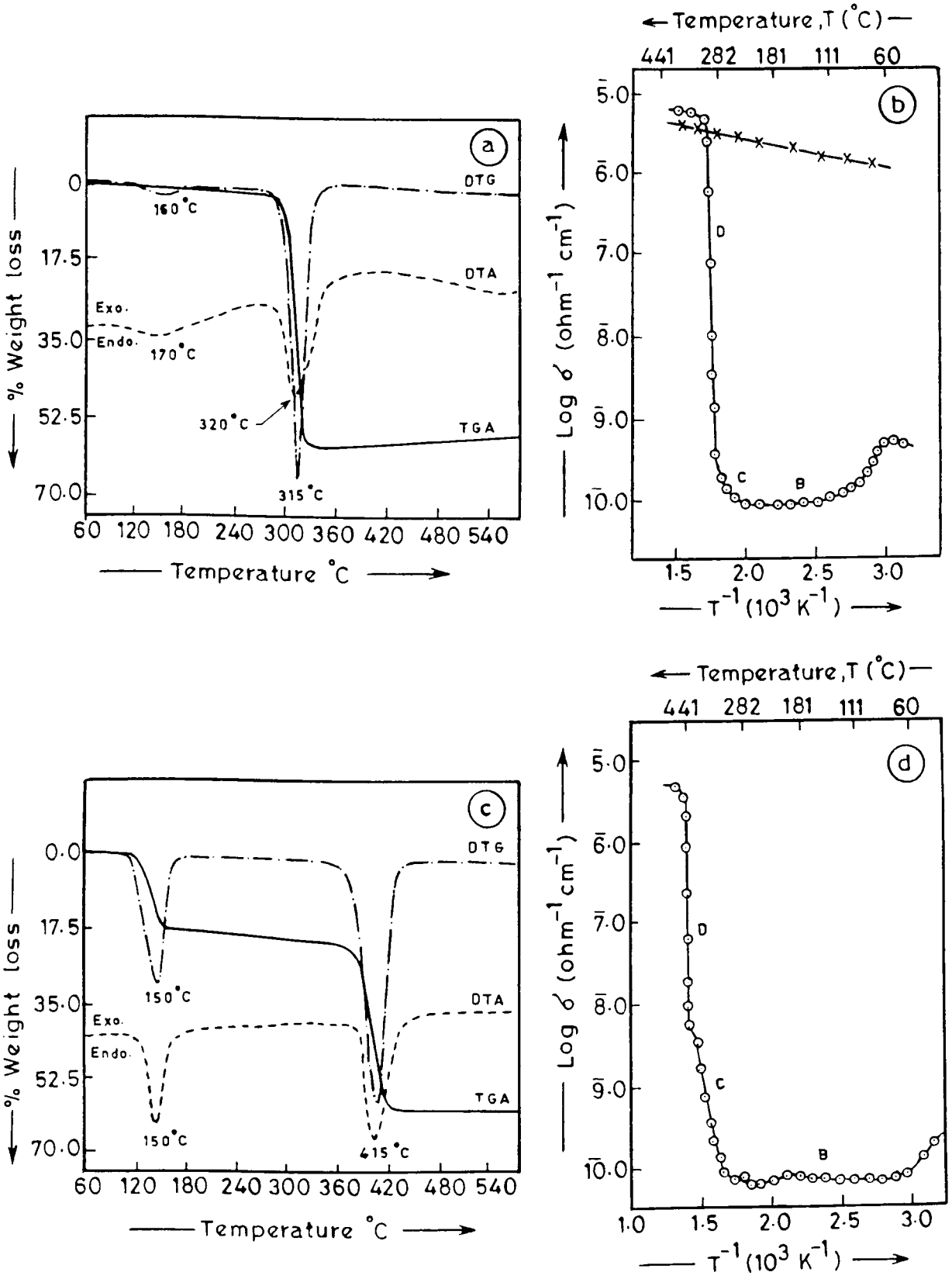

Fig. 5 Thermal decomposition in a dynamic nitrogen atmosphere : (a) TGA, DTG and DTA curves for $CuC_2O_4 \cdot H_2O$; (b) Plot of log σ vs. T^{-1} for $CuC_2O_4 \cdot H_2O$: ⊙ , during decomposition; x, cooling cycle; (c) TGA, DTG and DTA curves for $ZnC_2O_4 \cdot 2H_2O$; (d) Plot of log σ vs. T^{-1} for $ZnC_2O_4 \cdot 2H_2O$.

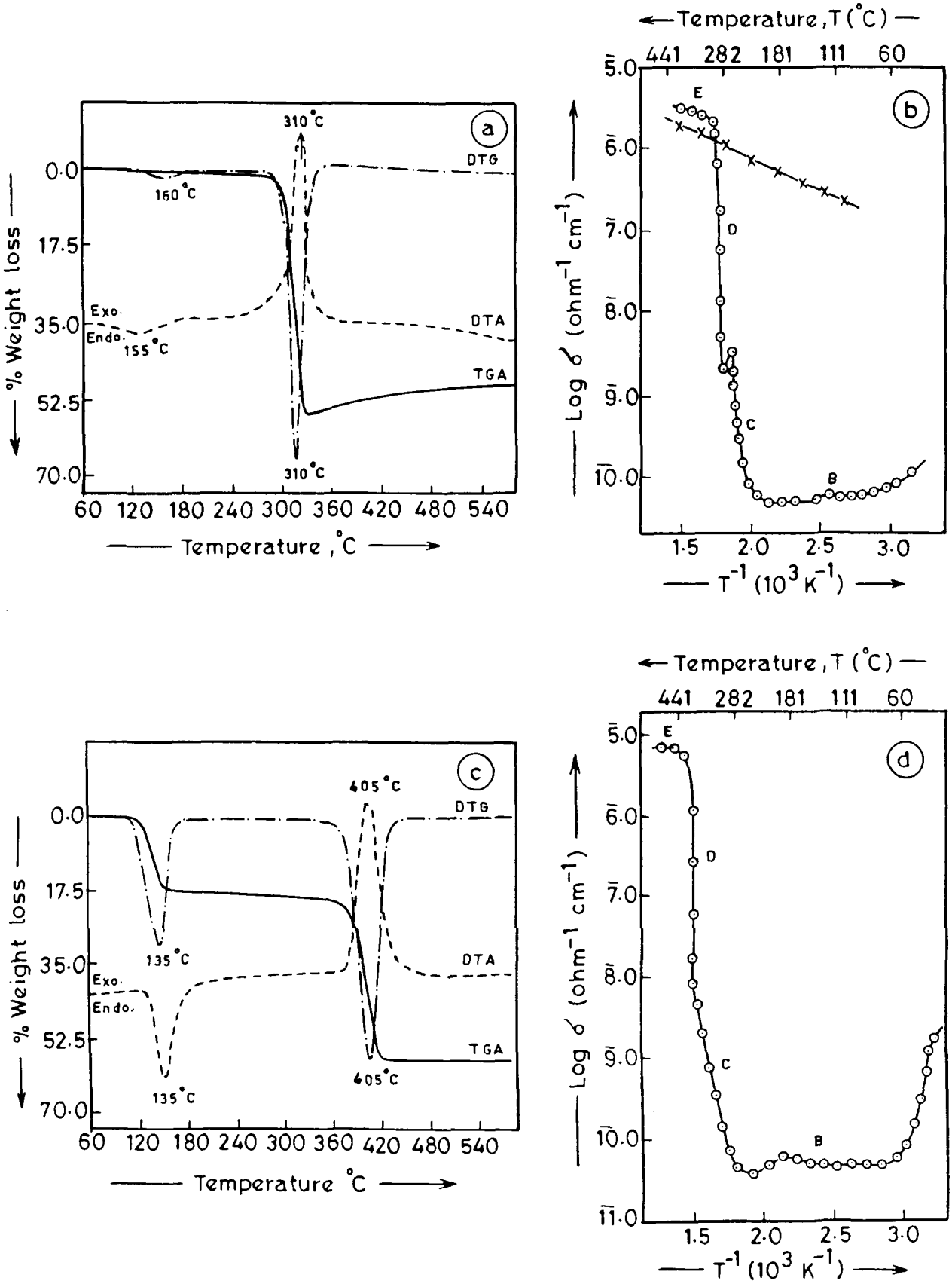

Fig. 6 Thermal decomposition in a dynamic air atmosphere.
(a) TGA, DTG and DTA curves for $CuC_2O_4 \cdot H_2O$;
(b) Plot of log σ vs. T^{-1} for $CuC_2O_4 \cdot H_2O$:
(c) TGA, DTG and DTA curves for $ZnC_2O_4 \cdot 2H_2O$:
(d) Plot of log σ vs. T^{-1} for $ZnC_2O_4 \cdot 2H_2O$.